Available online at www.sciencedirect.com
ScienceDirect
Journal of Power Sources 170 (2007) 101–110
JOURNAL OF POWER SOURCES
www.elsevier.com/locate/jpowsour

Numerical analysis of electrochemical characteristics and heat/species transport for planar porous-electrode-supported SOFC

Yuzhang Wang [a,b,*], Fumihiko Yoshiba [b], Takao Watanabe [b], Shilie Weng [a]

[a] *School of Mechanical Engineering, Key Laboratory for Power Machinery and Engineering of Ministry of Education, Shanghai Jiao Tong University, 800 Dong Chuan Road, Shanghai 200240, PR China*
[b] *Energy Engineering Research Laboratory, Central Research Institute of Electric Power Industry, 2-6-1 Nagasaka, Yokosuka, Kanagawa 240-0196, Japan*

Received 2 February 2007; received in revised form 29 March 2007; accepted 3 April 2007
Available online 10 April 2007

Abstract

In this work, a fully three-dimensional mathematical model for planar porous-electrode-supported (PES) solid oxide fuel cell (SOFC) has been constructed to simulate the steady state electrochemical characteristics and multi-species/heat transport. The variation of chemical species concentrations, temperature, potential, current and current density for two types of PES-SOFC developed by central research institute of electric power industry (CRIEPI) of Japan are studied in the co-flow pattern. In the numerical computation, the governing equations for continuity, momentum, mass, energy and electrical charge conservation are solved simultaneously using the finite volume method. Activation, ohmic, and concentration polarizations are considered as the main sources of irreversibility. The Butler–Volmer equation, Ohm's law, and Darcy's gas model with constant porosity and permeability are used to determine the polarization over-potential, respectively. The output voltages measured in experiments and calculated using the above models agree well. For the cell using the same material and manufacturing process, the results show the type-II PES-SOFC is with better performance. However, the electrolyte of type-II PES-SOFC should be with higher maximum ionic conductivity. Furthermore, these results will be used to evaluate the overall performance of a PES-SOFC stack, and to significantly help optimize their design and operation in practical applications.

Keywords: SOFC; Heat/mass transfer; Electrochemical reaction; Performance

1. Introduction

Solid oxide fuel cells (SOFC) are the basis of a promising technology for the high-efficiency conversion of hydrocarbon fuels to electric energy, and currently are considered one of the most promising type fuel cells used as a power source for stationary or distributed power plants [1,2]. SOFCs operate at relatively high temperature, around 700–1000 °C for maintaining high oxygen-ion-conductive of solid oxide electrolyte. Such high temperature accelerates electrochemical reaction; therefore, they do not require precious metal catalysts to enhance the reaction [3,4]. Among fuel cells, SOFCs have a great advantage in fuel adaptability. They are less sensitive to fuel composition compared to other fuel cell system. Besides the reformed gas from external reformer, the anode feed can employ natural gas, LPG, methanol, or coal gasified gas through internal reforming on the anode side. Another attractive feature is SOFC also can be combined with other power generation systems (e.g., gas turbines) to achieve high overall electrical power generation efficiency due to the high working temperature.

SOFCs usually consist of an interconnect structure and a three-layer region composed of two porous ceramic electrodes (anode and cathode), and a dense, gas-tight, oxygen-ion-conducting electrolyte. Planar and tubular geometries are the two popular designs for SOFCs. The technique of designing and manufacturing of tubular type SOFC is relatively mature [1,5]. However, planar type design has received much attention recently, because it is simpler to fabricate and easier to be made into various shapes than other type designs. Besides, planar type SOFC offers higher power density relative to tubular

* Corresponding author. Permanent address: School of Mechanical Engineering, Key Laboratory for Power Machinery and Engineering of Ministry of Education, Shanghai Jiao Tong University, 800 Dong Chuan Road, Shanghai 200240, PR China. Tel.: +86 21 6407 1386; fax: +86 21 6447 0679.
E-mail address: yuzhangwang@yahoo.com.cn (Y. Wang).

0378-7753/$ – see front matter © 2007 Elsevier B.V. All rights reserved.
doi:10.1016/j.jpowsour.2007.04.004

Nomenclature

A	area (m^2)
d_P	pore diameter in porous medium (m)
$D_{i,e}$	overall effective diffusion coefficient of species i ($m^2\,s^{-1}$)
D_{ij}	binary mass diffusion coefficient of a mixture species i and j ($m^2\,s^{-1}$)
$D_{i,m}$	mass diffusion coefficient for species i in the mixture ($m^2\,s^{-1}$)
D_K	Knudsen diffusion ($m^2\,s^{-1}$)
E_{TPB}	electromotive force (V)
F	Faraday's constant: 96,487 C mol^{-1}
ΔG	Gibb's free energy change ($J\,kg^{-1}$)
H	total enthalpy ($J\,kg^{-1}$)
ΔH	enthalpy change of the reaction ($J\,kg^{-1}$)
i	current (A)
j	current density ($A\,m^{-2}$)
j_0	exchange current ($A\,m^{-2}$)
k	turbulent kinetic energy ($m^2\,s^{-2}$)
Kn	Knudesen number $Kn = \lambda_f/d_P$
M	molecular weight ($kg\,kmol^{-1}$)
n_e	number of electrons
P	pressure (Pa)
$P_{i,TPB}$	the ratios of partial pressure over the standard state pressure of 1.013×10^5 Pa at the electrolyte/electrode interface $i \in \{H_2, H_2O, O_2\}$
R	universal gas constant ($J\,kg^{-1}\,K^{-1}$)
R_{ohm}	ohm resistance (Ω)
S_ϕ	source or sink
ΔS	entropy change of the reaction ($J\,kg^{-1}\,K^{-1}$)
T	temperature (K)
$\bar{U}$	velocity ($m\,s^{-1}$)
U_f	fuel utilization factor
V	potential (V)
V^c, V^a	electrical potential at anode and cathode, respectively (V)
x	width direction of the cell
X_i	molar fraction of species i ($kmol\,kmol^{-1}$)
y	thickness direction of the cell
Y	mass fraction of species ($kg\,kg^{-1}$)
z	length direction of the cell

Greek symbols

α	electron transfer coefficient (usually taken to be 0.5)
Γ_ϕ	diffusion coefficient ($kg\,m^{-1}\,s^{-1}$)
δ	thickness (m)
ε	turbulent dissipation rate ($m^2\,s^{-3}$)
ε_P	porosity of porous medium
η^{act}	over-potential incurred by the activation polarization (V)
η^{ohm}	over-potential incurred by the ohmic polarization (V)
κ_P	permeability of porous medium
λ	thermal conductivity ($W\,m^{-1}\,K^{-1}$)
λ_f	mean free path length (m)
ν	special Fuller et al. diffusion volume
ρ	density ($kg\,m^{-3}$)
ρ_i	resistivity (Ω m)
τ_P	tortuosity of porous medium

Subscripts

ca	cathode
ele	electrolyte
f	fuel
g	gas
IC	inter-connector
Ref	reference
s	porous solid

Superscripts

a	anode
c	cathode
e	electrolyte

type SOFC, which is ascribed to low electrical resistance due to shorter current paths.

In SOFC cell, the oxygen ions formed at the cathode migrate through the electrolyte to the anode/electrolyte interface where they react with the hydrogen and carbon monoxide contained in the fuel, producing water and carbon dioxide while releasing electrons that flow via an external circuit to the cathode/electrolyte interface [6]. SOFC system involves complex multi-component transport, chemical, and electrochemical processes, with its operating performance strongly affected by corresponding transport resistances and activation barriers [7]. Transport resistances of gas-phase species in the porous electrode and oxygen ions in the electrolyte, as well as the activation energy barriers for electrochemical reactions can result in various polarizations. They are represented as concentration, activation, and ohmic over-potentials. These various polarizations are functions of both operating conditions and physical properties of cell's components. The operating conditions include temperature, pressure, and fuel and oxidizer concentrations. The cell properties involve materials, macro- and micro-structures of electrolyte and composite electrodes, which include the porosity, tortuosity, permeability, and thickness of anode and cathode, the ionic conductivity and thickness of electrolyte, and the active area and activity of electrode–electrolyte interface.

A goal for SOFC is to develop economically acceptable systems. It is expected that the capital costs can be lowered through advancement in cell manufacturing and cell design. An increase in power density is a major technical contribution to further cut costs. To understand these various resistances, optimize the cell design, and enhance the cell performance, parametric studies for these various polarizations in the electrolyte and composite electrodes have been widely made through experiments [8,9], theoretical analysis [2,5,7,10,11], and numerical simula-

tion [1,3,12]. Experimental approaches would be very costly and time consuming. In addition, it would be very difficult to measure directly the detailed profile of chemical species, current, electric potential, etc. in the cell. However, the three-dimensional numerical simulation, based on commercial computational fluid dynamic (CFD) code and a user defined routine for dealing with electrochemical processes, can provides a better understanding of main phenomena that govern fuel cell performance [13], for example, the cell internal temperature and flow composition profiles, fuel and oxidant utilization, cell power output and cell voltage or current output.

In this work, based on commercial CFD software (CFX4.4) and a routine developed by ourselves and used to calculate the mass diffusion and heat transfer in the porous eletrodes for PES-SOFC cell, the electrochemical processes and the current field, a fully three-dimensional mathematical model for planar PES-SOFC has been constructed to simulate the flow, heat and mass transfer, and the electrochemical performance of two types of PES-SOFCs. The more detailed spatial variation of chemical species, local over-potential, electric potential and current density are obtained. These results will be used to evaluate the overall performance of the PES-SOFC stack, and to significantly help optimize their design and operation in practical applications.

2. Computational model

The schematic views of two types of new planar PES-SOFC simulated are shown in Fig. 1. The layer of electrolyte is laminated onto the diffusible porous electrode. In a practical planar SOFC stack, many planar cells are mounted in a container. For most of the planar cells mounted in serial way, each of them is connected by two others. Therefore, it is possible, and very likely, that most of the single planar SOFCs work under the same operating condition. This allows us to obtain results that are very useful for evaluating the performance of a cell stack, through analysis of heat/mass transfer and electrochemical performance of one single cell and its controllable area. In SOFC cell, the fluid consists of multiple components, oxygen and nitrogen in the cathode channel and hydrogen and water vapor in the anode channel. The heat and mass transfer are coupled with each other.

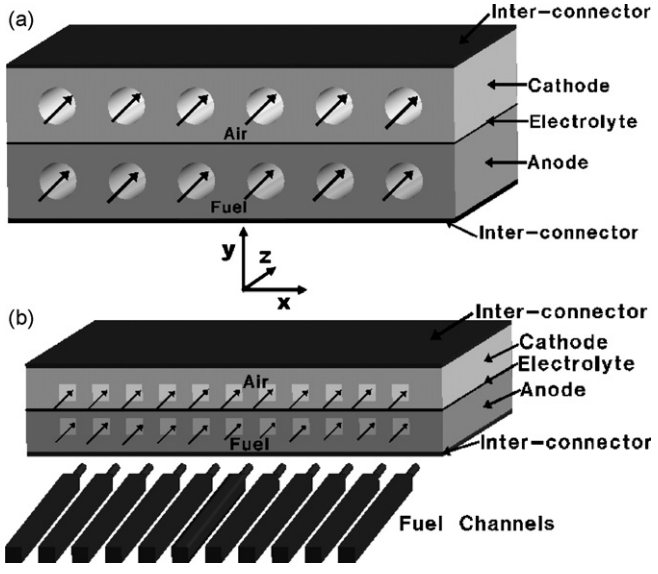

Fig. 1. Schematic view of two types of planar PES-SOFC: (a) type-I and (b) type-II.

2.1. Flow and heat/mass transfer

The basic set of equations for flow and heat/mass transfer comprises the equations for conservation of mass, momentum, energy and concentration, known as the three-dimensional Navier–Stokes equations. The effect of turbulence is represented by the $k-\varepsilon$ model. In this model, wall functions are used to resolve the flow near wall surfaces. The following time-averaged equations are used for steady state in compressible gases [14]:

$$\nabla \cdot (\rho \bar{U} \phi - \Gamma_\phi \nabla \phi) = S_\phi \tag{1}$$

where ϕ represents $\bar{U}$, k and ε, H and Y.

The model commonly used for flow in porous medium is a generalization of the Navier–Stokes equations and Darcy's law with constant porosity and permeability. Mass diffusion coefficients are required whenever species transport equations in multi-component flows are solved. Diffusion in porous medium is usually described by molecular diffusion or Knudsen diffusion. Knudsen diffusion occurs when the diameter pores in the porous mediums are small compared with the mean free path of the gas molecules, i.e. Knudsen number $Kn \gg 1$. Molecular diffusion occurs when the pore diameter is large compared with the mean free path of the gas molecules, i.e. $Kn \ll 1$. For SOFCs, both Knudsen and ordinary diffusion processed have to be considered since, in general, $Kn \approx 1$. The mass diffusion coefficient for species i in the mixture is computed as

$$D_{i,\mathrm{m}} = \frac{1 - X_i}{\sum_{j.j \neq i} (X_j / D_{ij})} \tag{2}$$

The binary diffusion coefficient D_{ij} of a mixture species i and j is computed using the Fuller et al. expression [15]:

$$D_{ij} = \frac{0.0143 T^{1.75}}{P M_{ij}^{1/2} [v_i^{1/3} + v_j^{1/3}]^2} \tag{3}$$

where $M_{ij} = 2(1/M_i + 1/M_j)^{-1}$ and v can be found in literature [15].

For straight and round pores [16], Knudsen diffusion is given by

$$D_{\mathrm{K}} = \frac{1}{3} d_{\mathrm{P}} \sqrt{\frac{8RT}{\pi M_i}} \tag{4}$$

Due to the pore's tortuous nature and pore constrictions, the diffusivity is corrected by tortuosity factor, τ_{P}, and porosity of porous medium, ε_{P}. The tortuosity factor accounts for both the effects of altered diffusion path length and changing cross-sectional area in constrictions. Zhang and Liu [17] proposed a new way to predict tortuosity in catalyst pellets based on fractal

Table 1
Physical properties of fuel cell components

	Type I	Type II
Geometry parameters		
Length (m)	60×10^{-3}	
Width (m)	60×10^{-3}	50×10^{-3}
Anode thickness (m)	10×10^{-3}	5×10^{-3}
Cathode thickness (m)	10×10^{-3}	5×10^{-3}
Electrolyte thickness (m)	0.05×10^{-3}	
Inter-connector thickness (m)	0.5×10^{-3}	
Material properties		
Thermal conductivity of anode ($W\,m^{-1}\,K^{-1}$)	6.23	
Thermal conductivity of cathode ($W\,m^{-1}\,K^{-1}$)	9.6	
Thermal conductivity of electrolyte ($W\,m^{-1}\,K^{-1}$)	2.7	
Thermal conductivity of inter-connector ($W\,m^{-1}\,K^{-1}$)	9.6	
Electric resistivity of anode ($\Omega\,m$)	$2.98 \times 10^{-5} \exp(-1392/T)$ [10]	
Electric resistivity of cathode ($\Omega\,m$)	$8.11 \times 10^{-5} \exp(600/T)$ [10]	
Ionic resistivity of electrolyte ($\Omega\,m$)	$2.94 \times 10^{-5} \exp(10{,}350/T)$ [10]	
Electric resistivity of inter-connector ($\Omega\,m$)	6.41×10^{-8} [3]	
Porosity of anode	0.38	
Porosity of cathode	0.5	
Permeability of anode	1.0×10^{-12}	
Permeability of cathode	1.0×10^{-12}	
Tortuosity of anode	1.5	
Tortuosity of cathode	1.5	
Pore diameter of anode	2.0×10^{-6}	
Pore diameter of cathode	2.0×10^{-6}	

geometries; a hard spheres model is often used for determining tortuosity. The accurate determination of this parameter is out of the scope of this paper and the measured values in Table 1 were used instead. The overall effective diffusion coefficient is given by [16]:

$$D_{i,\mathrm{e}} = \frac{\varepsilon_\mathrm{P}}{\tau_\mathrm{P}} \left(\frac{1}{D_{i,\mathrm{m}}} + \frac{1}{D_\mathrm{K}} \right)^{-1} \tag{5}$$

In order to take into account the heat conduction of porous solid, the effective thermal conductivity in the porous medium is computed by, as the volume average of the fluid conductivity and the solid conductivity:

$$\lambda = \varepsilon_\mathrm{P} \lambda_\mathrm{g} + (1 - \varepsilon_\mathrm{P}) \lambda_\mathrm{s} \tag{6}$$

where λ_g is the thermal conductivity of multi-component mixture, and its computational formula and coefficient can be found in literature [15]. λ_s is isotropic constant and its measured values are listed in Table 1.

In addition, there is large resistance of flow in the porous medium. The isotropic linear resistance tensor is proportional to the inverse of the permeability κ. The resistance force, i.e. body force, is the source of momentum equation.

2.2. Electrochemical model

The electrochemical model calculates the current power output and the molar compositions of cathode and anode flows for each control volume. For clarity and comparing with the experimental results, the calculating conditions are the same as the experimental conditions. The fuel consists of H_2 and H_2O on the anode side and the oxidizer (air) is modeled as an O_2/N_2 mixture on the cathode side. Fuel and air run in a co-current flow. The electrochemical reaction occurring at the interface of cathode/electrolyte is

$$\mathrm{O_2} + 4\mathrm{e}^- \rightarrow 2\mathrm{O}^{2-} \tag{7}$$

Then, the oxygen ion is transported through the electrolyte and into the active anode. The electrochemical reaction occurring at the interface of anode/electrolyte is

$$\mathrm{H_2} + \mathrm{O}^{2-} \rightarrow \mathrm{H_2O} + 2\mathrm{e}^- \tag{8}$$

The electromotive force yielded by the oxidation of H_2 is a local quantity, as it depends on the gas composition and temperature, and can be determined by the well-known Nernst equation, as following [1]:

$$E_\mathrm{TPB} = \frac{-\Delta G}{2F} = \frac{-\Delta G^\circ}{2F} + \frac{RT}{2F} \ln \left(\frac{P_{\mathrm{H_2,TPB}} P^{0.5}_{\mathrm{O_2,TPB}}}{P_{\mathrm{H_2O,TPB}}} \right) \tag{9}$$

In the electrochemical reaction proceeding, the changes of chemical enthalpy at temperature T, ΔH, entropy, ΔS, and Gibb's free energy, ΔG, have the thermodynamic relationship.

$$\Delta G = \Delta H - T\Delta S \tag{10}$$

Concentration over-potentials appear when the mass transport hinders the electrode reaction. Concentration polarization becomes an important loss at high current densities and small fuel concentrations ($U_\mathrm{f} \geq 80\%$). The main factors that contribute to concentration polarization are the diffusion of gases through the porous media and solution dissolution of reactants and products. Along with the consumption and production of the gas

species in fuel and air flows, the molar fraction of the reactants and products from the electrochemical reactions also vary in the flow stream of fuel and air. In Eq. (9), the Nernst electromotive force obtained includes the over-potential incurred by the component diffusion, due to using the species concentrations at the three-phase boundaries, i.e. considering the mass diffusion of multi-component flow in porous medium. This yields the localized electromotive force, E_{TPB}, over the electrolyte layer, which yields the localized ionic transfer rate through the electrolyte layer.

$$i = \frac{E_{\mathrm{TPB}} - \eta^{\mathrm{act}} - (V^{\mathrm{c}} - V^{\mathrm{a}})}{R^{\mathrm{e}}_{\mathrm{ohm}}} \tag{11}$$

2.2.1. Activation polarization

Activation polarization is controlled by the electrode kinetics at the electrode surfaces. This polarization is directly related to the activation barrier that must be overcome by the reacting species in order for the electrochemical reaction to occur. Activation over-potential, η^{act}, incurred by the activation polarization, reflects the kinetics of reactions and occurs at both anode and cathode. At high operating temperature, the electrode reaction is rapid and, as a result, the activation over-potential is usually small. However, as the operating temperature falls, it can become the most significant cause of voltage drop. It is often represented by the non-linear Butler–Volmer equation [8], which relates the current density drawn to the activation over-potential and, for a first order charge transfer controlled electrochemical reaction, is given by:

$$\frac{j}{j_0} = \exp\left(\alpha\frac{n_{\mathrm{e}}F\eta^{\mathrm{act}}}{RT}\right) - \exp\left(-(1.0-\alpha)\frac{n_{\mathrm{e}}F\eta^{\mathrm{act}}}{RT}\right) \tag{12}$$

where j_0 the exchange current density, given by [8]:

$$j^{\mathrm{a}}_0 = 5.5\times10^8\left(\frac{P_{\mathrm{H_2}}}{P_{\mathrm{Ref}}}\right)\left(\frac{P_{\mathrm{H_2O}}}{P_{\mathrm{Ref}}}\right)\exp\left(-\frac{100\times10^3}{RT}\right) \tag{13}$$

$$j^{\mathrm{c}}_0 = 7.0\times10^8\left(\frac{P_{\mathrm{O_2}}}{P_{\mathrm{Ref}}}\right)^{0.25}\exp\left(-\frac{120\times10^3}{RT}\right) \tag{14}$$

The non-linear Butler–Volmer equation is solved numerically using the Newton–Raphson method in this work. The computational accuracy is 1.0×10^{-6}.

2.2.2. Ohmic losses

Ohmic losses are caused by resistance to conduction of ions (through the electrolyte) and electrons (through the electrodes and inter-connector) and by contact resistance between cell components. This voltage drop is important in all types of cells and is essentially linear and proportional to current density. Because the ionic flow in the electrolyte and the electronic flow in the electrodes obey Ohm's law, ohmic losses can be expressed by:

$$\eta^{\mathrm{ohm}} = R_{\mathrm{ohm}} i \tag{15}$$

The ohm resistance is calculated according to the second Ohm's law:

$$R_{\mathrm{ohm}} = \rho_i\frac{\delta}{A} \tag{16}$$

where ρ_i is the corresponding material resistivity, calculated with temperature-dependent relation (Table 1).

In this work, the current calculation in the electrolyte is one dimension, along with the thickness direction, due to very small thickness, and it is three dimensions in the anode and cathode. Applying Kirchhoff's law of current, Eq. (17), the potential and current in each calculating volume are obtained:

$$\sum_{j=1}^{6} i_j = 0.0 \tag{17}$$

where $i_j = (V_j - V_P)/R_{j,P}$, P is the present calculating volume and j indicates six neighborhood volume at x-, y-, and z-axis. The difference between the current through every layer of the electrode and the given current is below 1.0×10^{-4}.

Since the potential difference between two inter-connectors is the cell terminal voltage, the potential at the outside surface of inter-connector in contact to the anode is assumed to be zero, thus the potential at the outside surface of inter-connector in contact with the cathode will be the terminal voltage of the fuel cell. Once all the local electromotive forces are obtained from Eq. (9), there are only two unknown condition, the total current flowing out from the cell and the potential at the inter-connector in contact with the cathode. Therefore, either must be specified as the initial condition. In the present work, the total current is specified according to the average current density and total reacting area of the cell.

3. Validity of models

The schematic view of experiment measurement of single cell for type-I PES-SOFC is shown in Fig. 2. In the figure, the Ref indicates the measuring reference point, the potentials on the cathode and the anode are measured at three measuring posi-

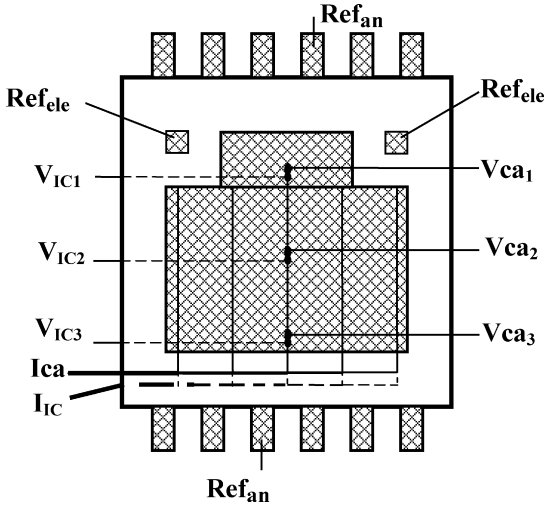

Fig. 2. Schematic view of experiment measurement.

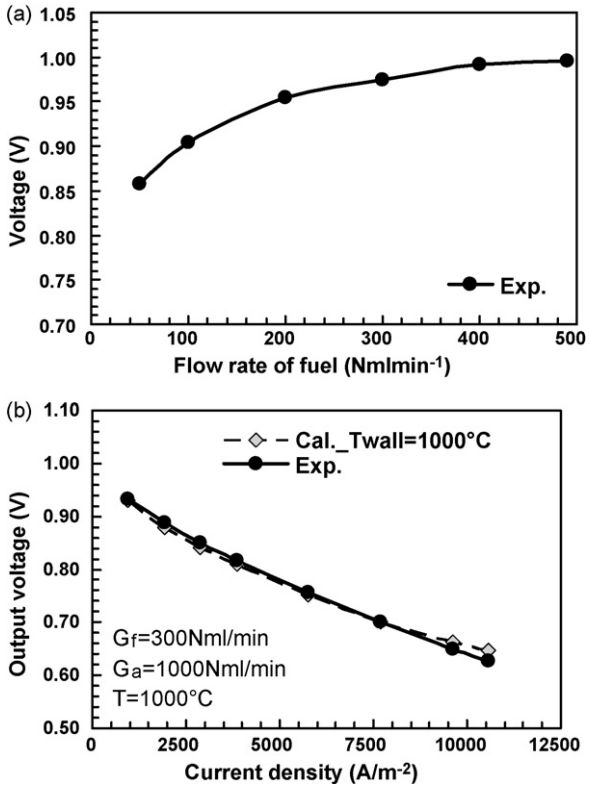

Fig. 3. Voltage (type-I cell): (a) voltage at open circuit and (b) output voltage of experiment and calculation.

tions, and the current is collected using the platinum wire. The experiment measurements are completed by Dr. Ito et al. (the researcher of materials science research laboratory of CRIEPI) under 1000 °C temperature.

The voltage at open circuit and the output voltage obtained from experiment and calculation at the same operating conditions and structure to the experiment equipment are given in Fig. 3. In Fig. 3a, it can be seen that the voltage at open circuit increases and trends to the constant, as the increasing of fuel flow rate. Then, the variation of the output voltage as a function of the current density under 300 N ml min^{-1} fuel and 1000 N ml min^{-1} air is measured. The output voltage decreases with the increasing of the current density. The output voltage of the calculation agrees well with that obtained for the experiment. This proves the above models used in the analysis are accurate and creditable, and is suitable to be used to analyze the performance of PES-SOFC cell [18].

4. Results and discussions

The measured physical properties of the cell components are listed in Table 1. The operating conditions are listed in Table 2. In the calculation, the fuel utilization is 80%, and the oxygen utilization is 10%. In the following, the more detailed spatial variation of temperature, chemical species, local overpotential, electric potential and current density are given. Due to most of single planar SOFC working under the same operating condition, the outside surfaces of two inter-connectors are specified to the periodic boundary. This means the heat exchange between the cells is the same. In the calculation, there is the no-electrochemical-reaction extend region (4 mm) at the inlet and outlet of cell. In the following figures, the midsection of pipe indicates the center-section of pipe on the porous electrodes, and the porous region indicates the cut-section between two pipes in the porous electrodes.

Table 2
Operating conditions

	Type I	Type II
Operating pressure (Pa)	1.013×10^5	1.013×10^5
Inlet temperature (°C)	1000	1000
Inlet mass flow rate of air (N ml min^{-1})	4775	4775
Inlet mass flow rate of fuel (N ml min^{-1})	130.6	108.8
Average current density (A m^{-2})	4000	4000
Electrochemical reaction area (m^2)	3.6×10^{-3}	3.0×10^{-3}
Fuel utilization (%)	80	80
Species molar fraction of fuel		
H_2	0.9578	0.9578
H_2O	0.0422	0.0422
Species molar fraction of air		
O_2	0.198	0.198
N_2	0.802	0.802

4.1. Distribution of temperature

Fig. 4 shows the temperature field for two types of PES-SOFC. On the whole, the fuel and air flow is progressively heated up by the heat generation due to the entropy change of the elec-

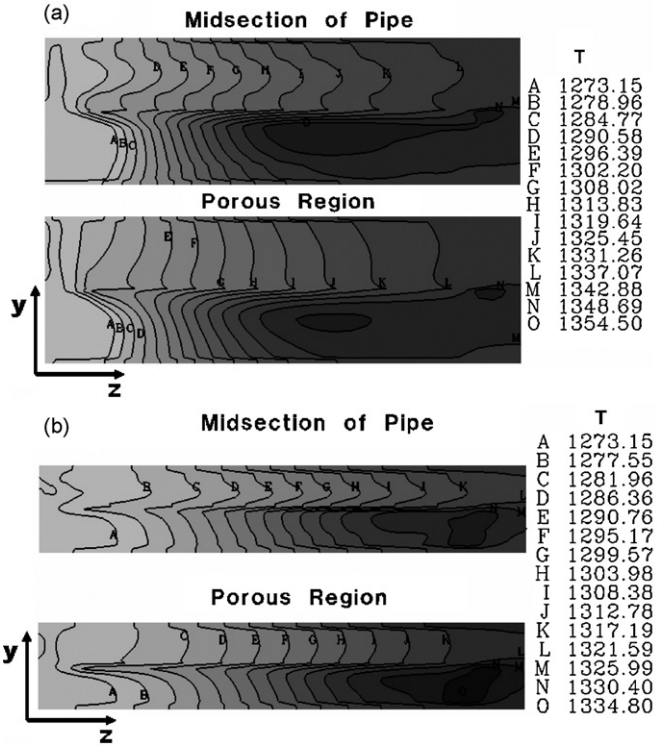

Fig. 4. Distribution of temperature: (a) type-I and (b) type-II.

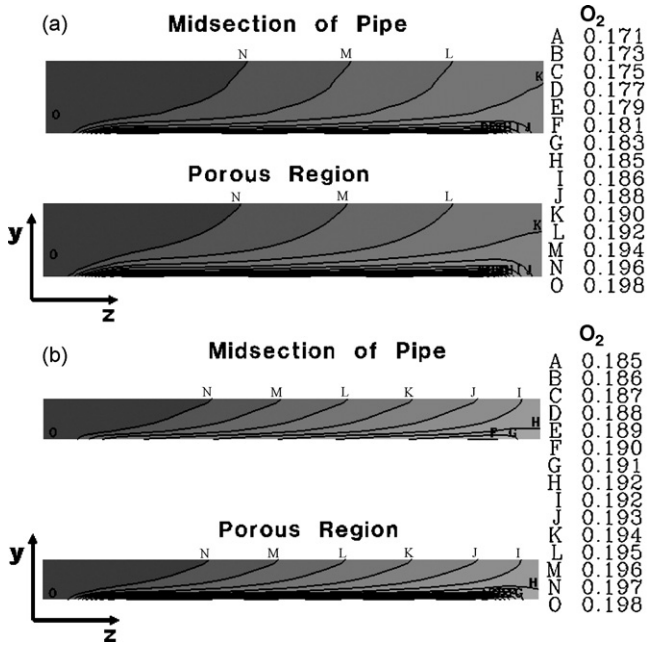

Fig. 5. Distribution of oxygen molar fraction in the cathode: (a) type-I and (b) type-II.

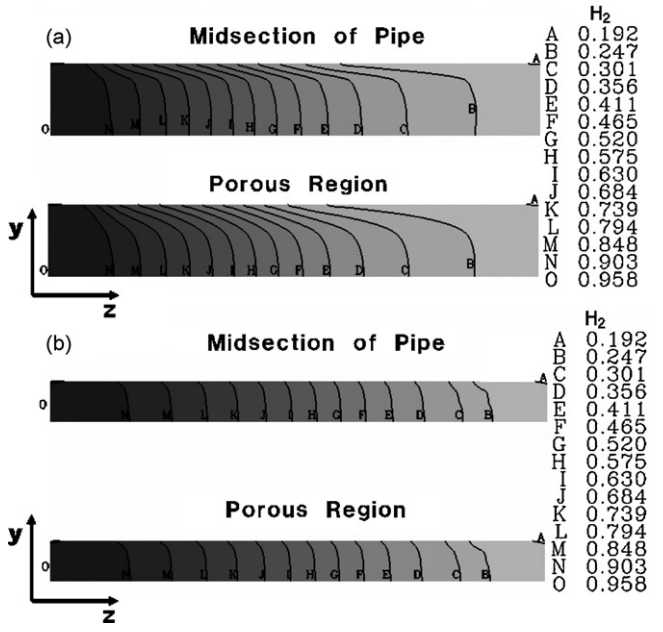

Fig. 6. Distribution of hydrogen molar fraction in the anode: (a) type-I and (b) type-II.

trochemical reaction at the interface of anode and electrolyte. The temperature of air flow in cathode channel is lower, especially in the pipe of cathode, due to its larger mass flow rate. In the anode channel, the fuel mass flow rate is very small, so its velocity is very low, especially in the porous medium due to large resistance force. In addition, the solid thermal conductivity of porous medium relative to the fuel flow is large. Therefore, the temperature distribution in the porous medium of anode channel is mainly determined by heat conduction. Due to the different thermal conductivity of different material of the cell components, there are larger temperature drops on the interface between different cell components.

From this flow arrangement, the hotspot temperature of the cell occurs in the output end of anode near the electrolyte. Nevertheless, the physical properties of the cell components, heat generation and input temperature and mass flow rate of air and fuel will collectively affect the temperature field in the fuel cell. Thus the hotspot position and temperature will depend on the operating condition of the fuel cell.

4.2. Distribution of species

Fig. 5 shows the distribution of oxygen molar fraction in the cathode channel. It is observed that the oxygen molar fraction decreases along the air flow direction due to the oxygen reduction reaction. The contour shape of oxygen also indicates a relatively large difference of oxygen molar fraction between the bulk flow and the cathode/electrolyte interface. Comparing Fig. 5a with b, the local molar fraction of oxygen in the cathode channel of type-II PES-SOFC is higher, due to the smaller distance between the bulk flow and the cathode/electrolyte interface. Fortunately, the mass flow rate of air is enough in order to control the cell temperature and prevent the cell broken. Thus, the mass transport resistance in the cathode channel might have an unimportant effect on the cell performance.

The distributions of hydrogen and water vapor molar fraction in the anode channel are shown in Figs. 6 and 7, respectively. Since the hydrogen consumption occurs at the interface of anode/electrolyte, the hydrogen molar fraction decreases along the fuel stream. Corresponding to this situation for hydrogen, the production due to the electrochemical reaction makes the water vapor increases gradually along the fuel stream. The shape of the

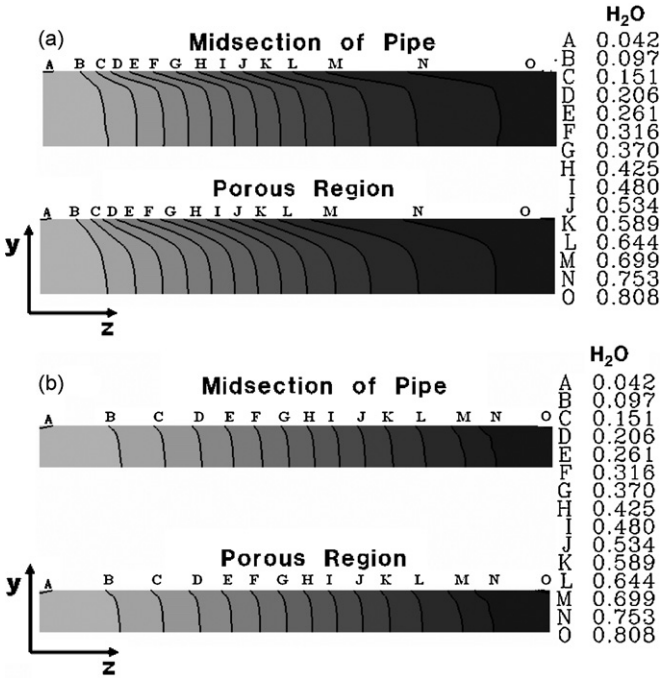

Fig. 7. Distribution of water vapor molar fraction in the anode: (a) type-I and (b) type-II.

contour lines of hydrogen and water vapor in the fuel channel is firstly very sharp and then relatively flat from the interface of anode/electrolyte to the interface of anode/inter-connector, and this also implies that species diffusion over-potential at the anode is larger than it at the cathode. Comparing Fig. 6a with b and Fig. 7a with b, the shape of the contour lines of hydrogen and water vapor in the fuel channel of type-II PES-SOFC is flatter relative to type-I PES-SOFC. This is owed to the smaller distance between the interface of anode/electrolyte and the pipe of porous medium. In a word, the mass transport resistance on the fuel channel might be dominant in lowering the cell performance, especially for high fuel utilization of the cell.

4.3. Distribution of current field

Fig. 8a and b shows the electric potential distributions on the mid-planes of the type-I and type-II PES-SOFC along the flow direction, respectively. In the porous medium of anode, due to the outside surface of inter-connector in contact to the anode assumed to be zero, the electric potential is the negative value, and it reduces from the outside surface of inter-connector to the interface of anode/electrolyte. Furthermore, due to the high electric conductivity of the anode material, its absolute values is small, the absolute maximum at the interface of anode/electrolyte, i.e. the ohmic over-potential of anode and inter-connector in contact to the anode is small. In the porous medium of cathode, the electric potential is the positive value, and it reduces from the interface of cathode/electrolyte to the outside surface of inter-connector in contact to the cathode. The

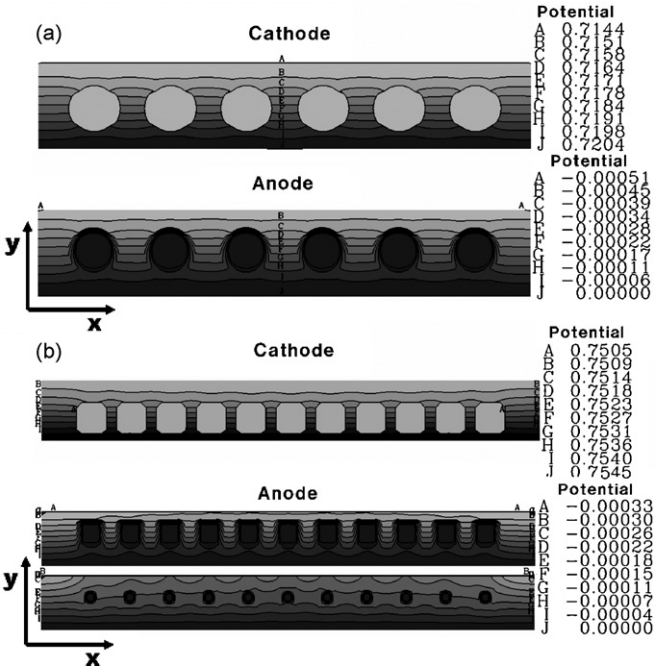

Fig. 8. Distribution of electric potential: (a) type-I and (b) type-II.

electric potential at the outside surface of inter-connector in contact to the cathode is the terminal voltage. At the region between two pipes of porous electrodes, the current through that area is relatively large which leads to more dense contour lines, i.e. there is a large drop of electric potential. It is also seen that the

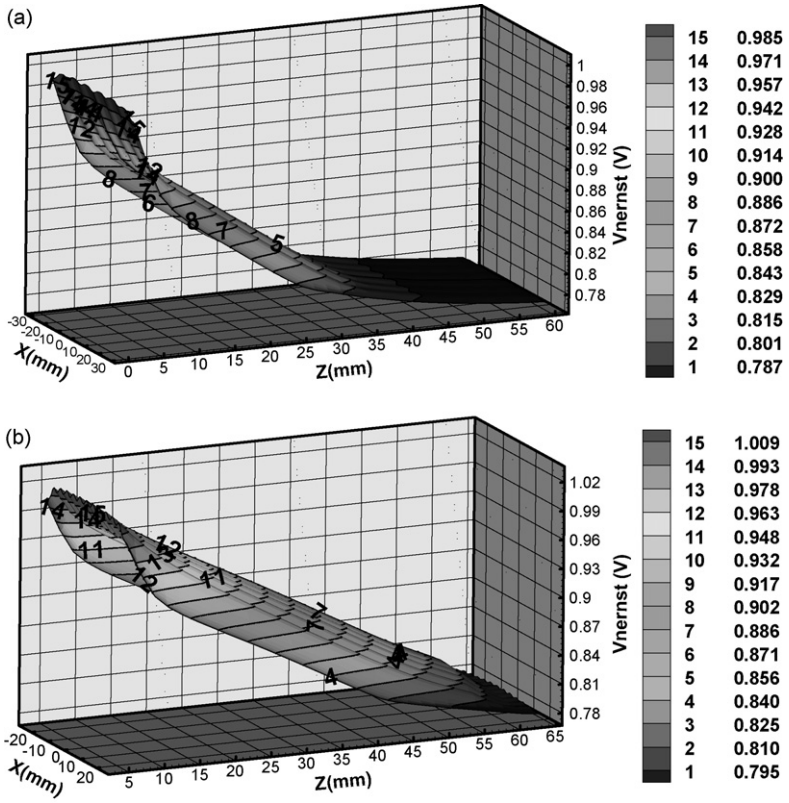

Fig. 9. Distribution of Nernst potential: (a) type-I and (b) type-II.

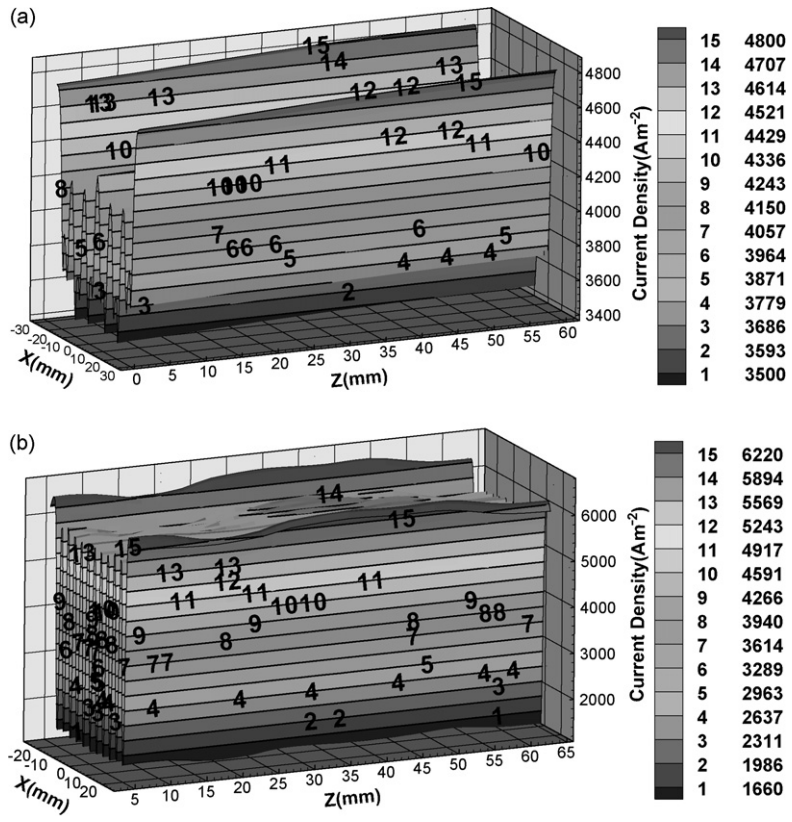

Fig. 10. Distribution of current density at the electrolyte: (a) type-I and (b) type-II.

cathode ohmic over-potential, the difference of electric potential between the interface of cathode/electrolyte and the outside surface of inter-connector in contact to the cathode, is larger than the anode ohmic over-potential. Comparing Fig. 8a with b, the ohmic over-potential of cathode and anode of type-II PES-SOFC is lesser than that of type-I PES-SOFC, due to the smaller thickness, and the terminal voltage of type-II PES-SOFC is larger than that of type-I PES-SOFC.

Fig. 9 shows the distribution of electromotive force, i.e. Nernst potential, taking into account the diffusion polarization. Due to the progressive decrease of hydrogen and oxygen concentration, the Nernst potential decreases along the flow direction (z-axis). The different diffusion of species in the pipe and porous region of the anode yields the Nernst potential presents the wave variation along x-axis. On the whole, the Nernst potential of type-II PES-SOFC is larger than that of type-I PES-SOFC, due to its smaller thickness of anode.

Fig. 10 shows the distribution of current (ionic transfer rate) density through the electrolyte. According to Eq. (11), the current density distribution is determined by many parameters, for example, temperature, species concentrations, potential of anode and cathode, activation over-potential, etc. As the temperature increases from inlet to outlet of the cell due to the electrochemical reaction, the ionic resistance of the electrolyte decreases. In addition, due to the larger heat exchange in the pipes of porous cathode, there is lower temperature at the regions of the electrolyte corresponding to these pipes, i.e. there is higher ionic resistance at these areas. Therefore, the ionic resistance of the electrolyte also presents the wave variation along x-axis, especially, for the type-I PES-SOFC. Because there is no the electronic conductor in the hollow pipes of porous electrodes, the potential and current in these pipes region is zero. The current accumulated at the interface of cathode/electrolyte moves around the hollow pipes region to the inter-connector. Conversely, the current in the anode moves form the inter-connector in contact to the anode to the interface of anode/electrolyte. The potential V^{c} of cathode near the electrolyte between these pipes and the electrolyte is higher in the cathode, whereas V^{a} is lower in the anode. Therefore, the current density also waves along the x-axis. There is lower value at the region corresponding to these pipes. Comparing Fig. 10a with b, the current density at the electrolyte of type-I PES-SOFC is evener than that of type-II PES-SOFC.

5. Conclusions

In the work, a fully three-dimensional numerical analysis of the fluid dynamics and electrochemical kinetics is conducted for two types of planar PES-SOFCs. Significant results about the spatial variation of temperature, species concentration, electric potential, etc. are presented. It is found that the fuel and air flow is progressively heated up along with the flow direction, and the hotspot locates at the end of the anode near the electrolyte, when the air and fuel stream is the co-flow. The mass transport resistance of species in the porous anode of type-I PES-SOFC under higher fuel utilization is dominant in lowering the

cell performance due to the larger thickness of anode. Under the same fuel utilization and average current density, the output electric potential of type-II PES-SOFC is higher than that of type-I PES-SOFC. This also means the cell performance of type-II PES-SOFC is better than that of type-I PES-SOFC. However, the electrolyte of type-II PES-SOFC should be with higher maximum ionic conductivity.

References

[1] P.W. Li, M.K. Chyu, J. Power Sources 124 (2003) 487–498.
[2] R.J. Kee, H. Zhu, D.G. Goodwin, J. Combust. Soc. Jpn. 47 (2005) 192–204.
[3] J.J. Hwang, C.K. Chen, D.Y. Lai, J. Power Sources 140 (2005) 235–242.
[4] Fuel Cell Handbook, 7th ed., Technical Report DOE/NETL 2004/1206, National Energy Technology Laboratory, Morgantown, WV, 2002, available at: http://www.detl.doe.gov.
[5] P. Aguiar, D. Chadwick, L. Kershenbaum, Chem. Eng. Sci. 57 (2002) 1665–1677.
[6] P. Aguiar, C.S. Adjiman, N.P. Brandon, J. Power Sources 138 (2004) 120–136.
[7] H.Y. Zhu, E.J. Kee, J. Power Sources 117 (2003) 61–74.
[8] P. Costamagna, A. Selimovic, M.B. Del, G. Agnew, Chem. Eng. J. 102 (2004) 61–69.
[9] P. Costamagna, K. Honegger, J. Electrochem. 145 (1998) 3995–4007.
[10] S. Campanari, P. Iora, J. Power Sources 132 (2004) 113–126.
[11] E.H. Pacheco, D. Singh, P.N. Hutton, N. Patel, M.D. Mann, J. Power Sources 138 (2004) 174–186.
[12] A.C. Burt, I.B. Celik, R.S. Gemmen, A.V. Sirnow, J. Power Sources 126 (2004) 76–87.
[13] V.A. Daniov, J. Lim, I. Moon, H. Chang, J. Power Sources 162 (2006) 992–1002.
[14] Y. Wang, Y. Li, S. Weng, Y. Wang, Energy 32 (2007) 852–860.
[15] B. Todd, J.B. Young, J. Power Sources 110 (2002) 186–200.
[16] S.H. Chan, K.A. Khor, Z.T. Xia, J. Power Sources 93 (2001) 130–140.
[17] B. Zhang, X. Liu, AIChE J. 49 (12) (2003) 3037–3047.
[18] Y. Wang, F. Yoshiba, T. Watanabe, Proceedings of the International Conference on Clean Coal Technology and Fuel Cells, Yokosuka, Japan, November 15–17, 2006, p. 115.